JOURNAL OF PROPULSION AND POWER
Vol. 26, No. 5, September–October 2010

Effects of Pylon-Aided Fuel Injection on Mixing in a Supersonic Flowfield

Hidemi Takahashi,* Qiuya Tu,† and Corin Segal‡
University of Florida, Gainesville, Florida 32611

DOI: 10.2514/1.48393

Previous analyses have shown that mixing can be enhanced using thin pylons that have only a negligible impact on pressure losses. In this study, helium and argon have been transversely injected into a Mach 1.6 airflow simulating a light and a heavy fuel injection behind a thin triangular pylon placed upstream, in the isolator. Penetration and mixing in the test section were observed at three cross sections, including the recirculation region and beyond, with planar laser-induced fluorescence. Results were compared to the no-pylon cases. The presence of the pylon resulted in improving both penetration and spreading of the jet and, at the same time, in lowering the concentration gradients in the recirculation region, which is an indication of improved flameholding ability.

Nomenclature

Ar	=	argon
A_j	=	injector area, mm^2
A_p	=	plume area, mm^2
$\bar{C}$	=	average of concentration, mol/m^3
C_{acetone}	=	acetone molar concentration, mol/m^3
C_i	=	instantaneous concentration, mol/m^3
C'_i	=	instantaneous concentration fluctuation, mol/m^3
C'_{rms}	=	standard deviation of concentration fluctuation
f	=	focus length, mm
H	=	step height, mm
He	=	helium
J	=	jet to crossflow momentum flux ratio
M	=	Mach number
P	=	static pressure, atm
P_{oj}	=	stagnation injection pressure, atm
P_s	=	static pressure at the entrance of isolator, atm
S	=	intensity signal
x	=	streamwise direction
y	=	transverse direction
z	=	spanwise direction

I. Introduction

THE short residence time in practical supersonic combustion systems, typically of the order of a few milliseconds, imposes severe requirement for mixing (and vaporization if liquid fuels are used) to ensure efficient heat release and positive net thrust generation [1]. The issue of mixing enhancement is therefore of particular interest for these devices.

Various types of fuel injection configurations and injector shapes have been studied for mixing enhancement mostly focused on changing the flowfield within the combustor [2,3]. Straight or swept ramps that produce near parallel injection have shown reasonable far-field mixing [4–6], although their near-field mixing performance falls below transverse injection alternatives. The ramp vortex shedding provides a means to lift the fuel from a low injection angle and promotes penetration into the core airstream. Because physical inflow ramps require cooling, especially in localized hot spots such as in recirculation regions, the aerodynamic ramp [7,8], or an angle-injection solution [9,10] from a flush wall have been suggested as noncooled injection configurations.

A solution that takes advantage of the high penetration of transverse injectors without the penalty of high pressure losses are the pylon-based injectors suggested by Vinogradov and Prudnikov [11]. It involves thin, swept pylons with the fuel injected transversely in the separated region behind them. The results showed that the penetration increase with these pylons was substantial. Livingston et al. [12] showed that thin pylons can be used with minimal pressure losses and applied this type of injection in an inlet, upstream of the isolator to provide additional mixing length. Hence, it is possible to achieve considerable penetration with relatively low dynamic pressure ratios, even less than unity, using this type of pylons. This is significant in particular when considering that in most cases normal injection from the wall requires dynamic pressure ratios of the order of 10–15 [13]. A review of thin pylons applications is given by Vinogradov et al. [14].

To increase the residence time and achieve a higher degree of mixing in the combustion chamber it may be useful to inject part of the fuel upstream, in the isolator, in the inlet or further upstream on the vehicle body. In this case a complex but more flexible system is obtained; the optimization of this system could result in multiple advantages including 1) mixing enhancement; 2) shorter isolator and combustor and, consequently, reduced weight and cooling loads; 3) a more flexible fuel control system, due to the possibility of distributing the fuel between the preinjection region and the combustor; and 4) the possibility of injecting combinations of liquid and gaseous fuels in different regions [1,15].

When the fuel is injected upstream, there is a danger of flashback due to fuel remaining in the boundary layer potentially causing upstream flame propagation. With the pylons described here penetration increases and the residual fuel in the boundary layer is avoided. Owens et al. [15], Shikhman et al. [16], Vinogradov et al. [17], and Guoskov et al. [18] showed in combustion experiments that fuel injection upstream of the combustion chamber was possible without flashback. The same is true for liquid-fuel injection, as shown by the experiments by Livingston et al. [12] where, in an inlet operating at $M = 3.5$, the pylon helped to remove the fuel entirely away from the wall. Most significantly, from the mixing enhancement point of view, the jet experienced an abrupt breakup and was carried into the inlet core airflow at the pylon height. Hence, the pylon's presence helped placing the fuel in a favorable mixing region.

More recently, Gruber et al. [19] confirmed these results evaluating pylon-aided fuel injection with three pylon geometries. In all cases the presence of the pylon resulted in improved fuel

Received 3 December 2009; revision received 21 June 2010; accepted for publication 23 June 2010.

*Postdoctoral Fellow, Mechanical and Aerospace Engineering. Member AIAA.
†Graduate Research Assistant, Mechanical and Aerospace Engineering. Student Member AIAA.
‡Associate Professor, Mechanical and Aerospace Engineering. Associate Fellow AIAA.

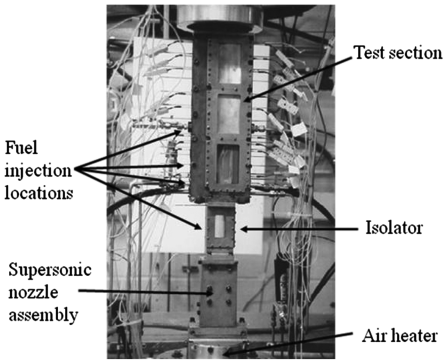

Fig. 1 Supersonic combustion facility.

penetration without leading to significant total-pressure-loss characteristics. Computationally, Pohlman and Greendyke [20] obtained similar results using five triangular pylons.

In the study described here, light (helium) and heavy (argon) gases were injected transversely through a circular injector in the base of the pylon located 10 steps ($10H$) upstream of the flameholding region in the isolator. Several dynamic pressure ratios were applied. The isolator entrance Mach number was 1.6. Penetration, spreading, and mixing were measured via acetone planar laser-induced fluorescence (PLIF) at three axial locations in the test section, beginning with the recirculation region. The results were then compared with the corresponding no-pylon cases. Considerable improvements in mixing have been observed when the pylons were present.

II. Experiment Facility and Technique

A. Facility

The facility used here has been described in detail elsewhere [21]. This continuously operating wind tunnel, shown in Fig. 1, is based on a vitiated heater electronically controlled by a hybrid fuzzy logic controller. The nozzles are interchangeable to provide a range of isolator's entrance Mach numbers from 1.6 to 3.6. All the experiments presented here were conducted at Mach 1.6 and stagnation temperature 300 K. The facility's stagnation pressure was maintained at 4.8 atm.

Both isolator and the test section have quartz glass windows for optical access. The isolator has a constant cross-sectional area of 25×25 mm^2. The combustion chamber has a rearward-facing step with height $H = 12.5$ mm acting as a quasi-two-dimensional flameholder.

B. Pylon Injector and Experimental Conditions

Gaseous helium (He) and argon (Ar) were used as injectants to simulate a light fuel (hydrogen) and a heavy fuel, e.g., propane, to evidence the effect of molecular weight. The fuel was transversely injected into the supersonic crossflow from a 1-mm-diam orifice located at $10H$ upstream of the step, in the isolator, as shown in Fig. 2. Two different stagnation injection pressures were applied: 2.4 and 5.1 atm. Both pylon and nonpylon configurations were evaluated. The pylon was designed, as shown in Fig. 2, to minimize the aerodynamic drag; hence, the thickness was selected as 2.3 times the injector diameter with swept leading edge and triangular cross section based on previous design recommendation [11].

C. Acetone PLIF

Figure 3 schematically illustrates the acetone PLIF system used for measurements. The fourth harmonic from a Spectra-Physics Nd:YAG laser (GCR-150) was used with a wavelength of 266 nm and output energy of 0.75 W at 10 Hz. The beam was expanded into a two-dimensional sheet of 50 mm wide and 0.5 mm thick. The optical path included three mirrors, two cylindrical convex lenses of $f = 100$ mm and 500 mm, and one cylindrical concave lens $f = -100$ mm, so that the flowfield could be probed with a vertical laser sheet. The fluorescence images were recorded using an intensified digital charge-coupled device camera with a 1024×1280 array and a Sigma 50-mm $f2.8$ camera lens. The camera gate was set to 10 ns to collect the acetone fluorescence's life time of 4 ns. The devices were synchronized by a pulse generator. A bandpass filter (335–610 nm) and a short-pass filter ($\sim$500 nm) were placed in front of the camera to eliminate elastic light reflections. The spatial resolution of the camera was 62.5, 104.2, and 63.3 μm/pixel for planes 1, 2, and 3, respectively. The injectant density change due to acetone seeding was estimated to be less than 1.4%, assuming saturated condition at the injector. Therefore, this level of acetone seeding caused a negligible influence on the injectant density.

The intensity of laser-induced fluorescence from the acetone molecule depends on the local temperature, pressure, and mole fraction, and the coexisting species and the intensity of the signal S was translated into the acetone molar concentration C_{acetone} (mol/m^3) [22]. The error was estimated to be 6.5% when assuming a linear relationship by the method described in [23]. Figure 4 shows the step and the location of three laser sheet planes. The injection was at $10H$ upstream of the step and the laser sheet planes were at $0.5H$, $2H$, and $10H$ downstream of the step, hence in the recirculation region close to the step, toward the end of the recirculation region (since the reattachment was at $2.7H$) and further downstream in the far field.

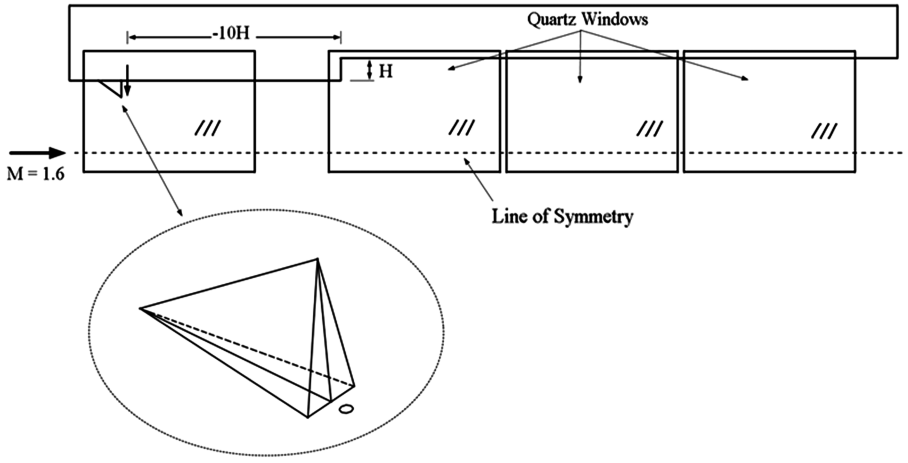

Fig. 2 Isolator and combustion chamber schematic and pylon geometry. The fuel was transversely injected into the supersonic crossflow from a 1-mm-diam orifice located at $10H$ upstream of the step, i.e., in the isolator. The pylon is 7.5 mm high and 2.3 mm wide at the base. Windows allow flow access for PLIF and visualization in the isolator and the test section.

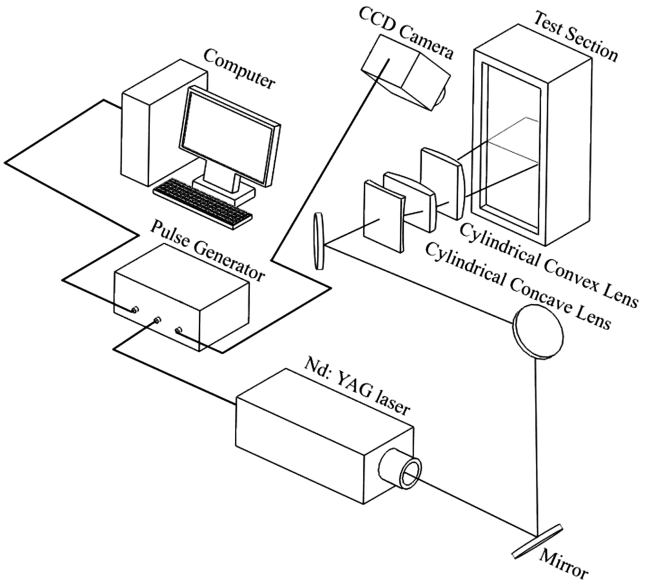

Fig. 3 Schematic of acetone PLIF measurement system. The laser beam was expanded into a two-dimensional sheet of 50 mm wide and 0.5 mm thick at three heights along the vertically oriented test section.

III. Results and Discussions

A. Schlieren Photograph and Pressure Distributions

Figure 5 is a schlieren photograph of the airflow before fuel injection showing the isolator and the combustion chamber. There are weak Mach waves in the isolator due to a slight misalignment of the nozzle and isolator interface. In the combustor the airflow expands around the step and reattaches at $2.7H$ [24]. The recirculation region formed behind the step receives different amounts of fuel, depending on the presence of fuel injection in the isolator in this case, or downstream as done in other configurations. The resulting composition has a critical effect in the flameholding ability [25].

The test section wall pressure distributions shown in Fig. 6a for He and Fig. 6b for Ar indicate that there is a pressure increase of 0.2 atm immediately behind the pylon and no difference downstream of the step. It should be noted that the isolator pressure rise is local, behind and aligned axially with the pylon, without effect on the rest of the flow [15], indicating that the presence of the pylon causes essentially no pressure loss.

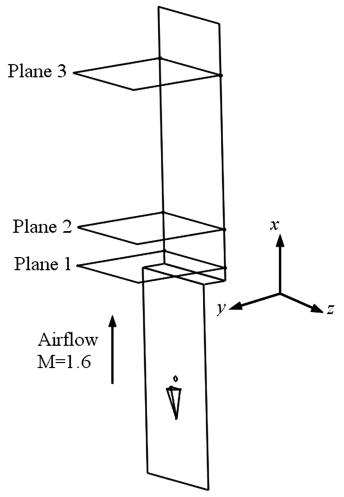

Fig. 4 Location of the selected flow planes. The injection was at $10H$ upstream of the step and the laser sheet planes were at $0.5H$, $2H$, and $10H$ downstream of the step. The x, y, and z axes correspond to the streamwise, transverse, and spanwise directions. The three planes investigated are in the recirculation region close the step, toward the end of the recirculation region (since the reattachment was at $2.7H$ downstream from the step) and further downstream in the far field.

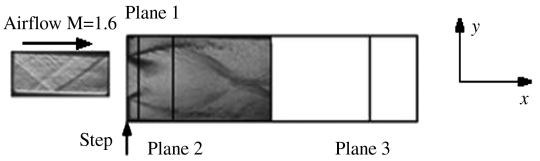

Fig. 5 Schlieren photograph of the airflow without injection or pylon [24]. The black lines indicate the positions of the laser sheet for subsequent PLIF.

B. PLIF Results

Instantaneous and ensemble-averaged images described below provide details of the flow structure, emphasizing the details of penetration and spreading, which are the two main factors influencing fuel–air mixing.

1. Instantaneous Structures

Figure 7 presents representative instantaneous PLIF images taken at the selected three planes for four cases, which correspond to $x/H = 0.5$, 2, and 10 downstream of the step; hence, the first two planes are in the recirculation region and the third is further downstream. In each image, the main flow direction is out of the paper plane, and the axes are normalized by the step height H. The origin is placed at the center of the duct in the y direction and at the step in the axial direction, x. The injection location is in the isolator at $z/H = 0$, $x/H = -10$, and $y/H = -1$. The LIF intensities are normalized by the maximum intensity in each plane. The highlighted white solid line shows the step. Because of symmetry, only half of the duct is shown in Fig. 7.

The instantaneous images show, to a certain extent, the turbulent structures, which include both the vortical structures and the flow turbulence effects. In the near field a compressibility effect is noted due to molecular weight differences creating a difference in the structure size. But in the far field the compressibility effect seems to weaken, because almost no difference in structure sizes is noted.

Without the pylon the fuel penetrates rapidly in the recirculation region through the shear layer, but remains confined to a small region. With the pylon the instantaneous structure is larger and it stretches in vertical direction while in nonpylon cases the plume occupies a smaller region, indicating less penetration and spreading. The structure due to the shear [26,27] effect is seen at the periphery of the jet plume. In some cases part of the plume is removed from the rest, as shown in plane 3 in Fig. 7c. Moreover, the jet plume often reaches the opposite wall for pylon-assisted cases. For the higher-molecular-weight injectant, i.e., argon, most of the injectant remains close to the injection wall, which is an effect of lower diffusion.

The instantaneous image results reveal the complex nature of the injectant/air interaction, which is principally responsible for mixing; they also indicate that highly intermittent and dynamic features still exist in the far field. The main effect of the pylon is to create the low-pressure region behind it, leading to increased penetration; however, as a secondary effect, weak vortical structures induced by the pylon help enhance spreading and mixing.

2. Ensemble-Averaged Structures

Figures 8–11 show ensemble-averaged PLIF images for each injectant and injection pressure, with plane 1, plane 2, and plane 3 shown from left to right. For each image 300 single-shot frames were used for averaging planes 1 and 2 and 600 frames were used for plane 3, since the latter showed weak intensities. The effects of injection pressure and molecular weight are described below.

a. Effect of Injection Pressure. Figure 8 shows the He injection with the pylon. At lower injection pressure, shown in Fig. 8a, for each plane the core of the plume is closer to the injection wall and the penetration is shorter than those in Fig. 8b, in which the pressure was higher. In planes 2 to 3 the spreading dominates, with

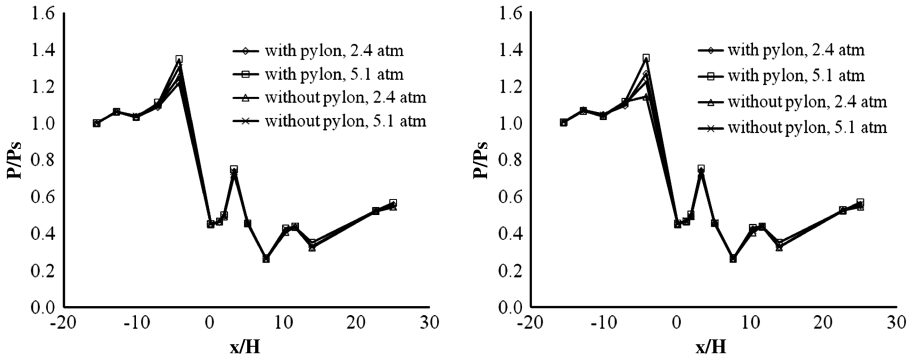

Fig. 6 Normalized pressure distribution at two different stagnation injection pressures. There is a slight pressure increase of 0.2 atm behind the pylon and no difference downstream of the step in the combustion chamber. This indicates that the presence of pylon causes no significant pressure loss.

little increase of penetration as the injection pressure is increased. In plane 1 the core of the jet approaches the chamber centerline, at $y/H = 0$. In plane 2 the core of the triangular-shaped plume with a wider spread is pushed toward the wall by the airflow expansion around the step and increases again after the reattachment point. As shown in plane 3, a characteristic shape with top central part penetrates far into the core flow with an even wider spread, almost reaching the sidewalls. The plume development for Ar injected behind the pylon, shown in Fig. 9, shows a similar trend as He: higher injection pressure enhances penetration with the plume shape changed from triangular in plane 2 to the widely spread shape in plane 3.

Without the pylon, at higher injection pressure He injection, Fig. 10 shows an elongated shape in plane 1 and becomes almost round further downstream. It is lifted from the injection wall with some increase of penetration to the step height and spreading, while at lower injection pressure a triangular-shaped plume appears in plane 1 and at the end of recirculation region. Further downstream it remains close to the injection wall, but it spreads more, reaching the sidewalls. Figure 11 shows the plume images of Ar without pylon, with a similar development as He; at higher injection pressure the spreading is narrower, but penetration is higher.

Penetration scales with the fuel-to-air momentum flux ratio [28] J; hence, higher injection pressure increases the penetration regardless of the presence of pylon. Although previous studies have shown that the presence of pylons reduces spreading [19], both penetration and spreading are increased here, and furthermore, penetration is increased at higher injection pressure. The additional effect on spreading is likely due to the presence of 3-D flow structure following expansion around the 2-D step as a result of the vortical motion induced by the presence of sidewalls.

b. Effect of Molecular Weight. When the pylon is present the jet plume axial development is similar for He and Ar with several notable differences. In plane 1 close to the step Ar penetrates less than He whereas in the far field, at plane 3, the penetration is much higher at lower injection pressure, as shown in Figs. 8 and 9. Without the pylon there is no penetration difference between the two injectants, as shown in Figs. 10 and 11, but Ar has a wider spreading and a larger plume area than He in every corresponding case. Thus, it appears that the molecular weight has only a small effect on the plume penetration in agreement with the observations of Portz and Segal [29] and Burger et al. [30], although the heavier injectant can enhance spreading even without the aid of the pylon.

3. Geometrical Features of Jet Plume

Figures 12–14 show certain salient features of the ensemble-averaged images including the plume area, penetration, and lateral spreading. The 10% contour of the maximum intensity was taken as the jet plume boundary. The plume penetration y was determined from the peak location of this contour, and the lateral spread Δz was determined from the widest extend of it; both were normalized by the step height. To avoid any noise in the data, the pixels inside the 30% contour were counted as the plume area normalized by the injector area.

In each case the plume area gradually became larger except for He from plane 2 to plane 3 at 2.4 atm with pylon and at 5.1 atm without pylon, as shown in Fig. 12. In the far field, at $20H$, helium spreading is considerable after the high penetration induced by the pylon presence, considerably more than Ar given the lower molecular weight. Much of the material has reached the walls that confine the further spreading of the injectant. Since the PLIF method has less accuracy close to the walls and the data in Fig. 12 are an average of a large number of images, the results indicate a trend different from that in the other curves; however, mixing is high in this case.

At higher injection pressure the plume area increased regardless of the pylon's presence, but with the pylon the increase was larger. The increase is most significant at higher injection pressure with pylon from plane 1 to plane 2. Figure 13 shows the plume penetration. For Ar the penetration was higher at higher injection pressure and the presence of pylon enhanced it. For He, except in the case with pylon, at higher injection pressure the penetration showed the same trend as Ar, while in other cases the penetration decreased from plane 2 to plane 3. This is due to the presence of the sidewalls at plane 3 that limit the plume spreading in the far field. For both injectants, with the pylon present the spreading was narrower than without the pylon. Helium penetration is very high when assisted by the pylon at both pressures. Further downstream, this very high plume penetration of He cannot be sustained when the injection pressure is low.

4. Statistical Analysis

Since the fluorescence signal represents the jet molar concentration, the spatial correlation of the PLIF signal fluctuations expresses the spatial extent of the turbulent scalar field. The single-time two-point spatial correlation analysis is useful to clarify the behavior of the turbulent structure [27,31]. The correlation coefficient $r(\Delta y, \Delta z)$ based on the concentration fluctuation is computed from Eq. (1):

$$\bar{C}(y,z) = \frac{1}{N}\sum_{i=1}^{N} C_i(y,z), \qquad C_i'(y,z) = C_i(y,z) - \bar{C}(y,z),$$

$$C'_{\mathrm{rms}}(y,z) = \sqrt{\frac{1}{N}\sum_{i=1}^{N} C_i'^2(y,z)}, \qquad i = 1,\ 2, \cdots, N \tag{1}$$

$$r(\Delta y, \Delta z) = \frac{\frac{1}{N}\sum_{i=1}^{N}[C_i'(y,z)\cdot C_i'(y+\Delta y, z+\Delta z)]}{C'_{\mathrm{rms}}(y,z)\cdot C'_{\mathrm{rms}}(y+\Delta y, z+\Delta z)}$$

where point (y, z) is the reference used for features correlation [32], $C_i(y,z)$ is the instantaneous concentration, $C_i'(y,z)$ is its fluctuation, $\bar{C}(y,z)$ is the average of concentration, $C'_{\mathrm{rms}}(y,z)$ is the standard deviation of concentration fluctuation, and Δy and Δz are the spatial differences in y and z directions, respectively. In the

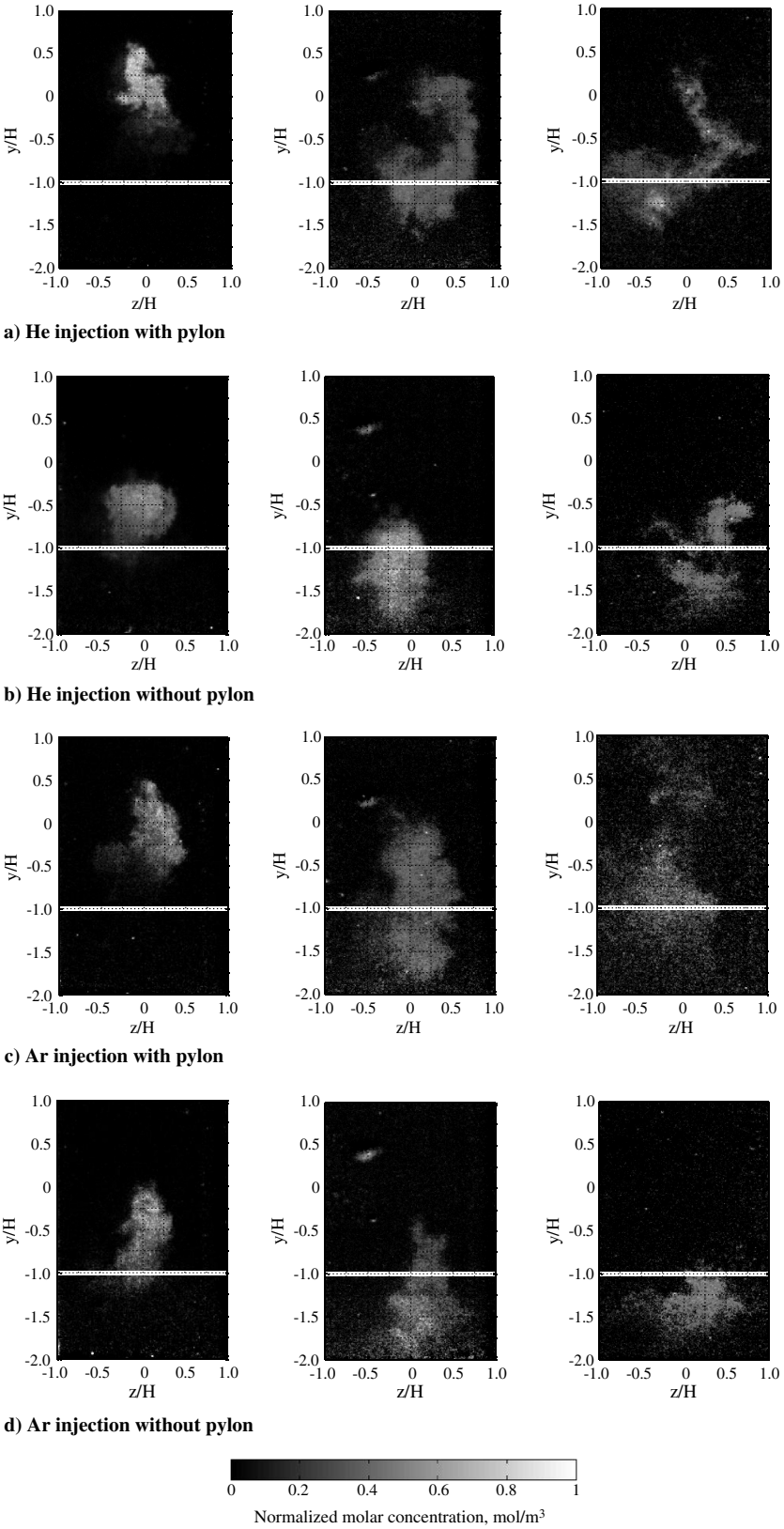

Fig. 7 Instantaneous end-view PLIF images in three measurement planes for four different injection cases: plane 1 (left), plane 2 (center), and plane 3 (right). Airflow direction is out of the paper plane, and the injection location is $z/H = 0$ and $x/H = -10$. The white solid line at $y/H = -1$ represents the step height.

present study, the significantly correlated region with a sample size N of 300 was chosen, where the absolute value of the correlation coefficient $|r| \geq 0.16$, as determined by statistical testing. In Fig. 15 each correlation map is depicted with the contour levels varying in increments of 0.1 in $0.2 \leq |r| \leq 1.0$. The line of $r = 0.16$, which indicates the boundary of the highly significantly correlated regions, is highlighted with a black solid line. The contours of 0.1 and 0.5 in averaged plume intensities are plotted as well, for reference. The reference points for calculating the correlation maps are the bottom edge of the 0.5 contour, since the concentration fluctuation is the most intensive on the 50% contour [31]. For correlation analysis of this end-view image, 300 single-shot images were used.

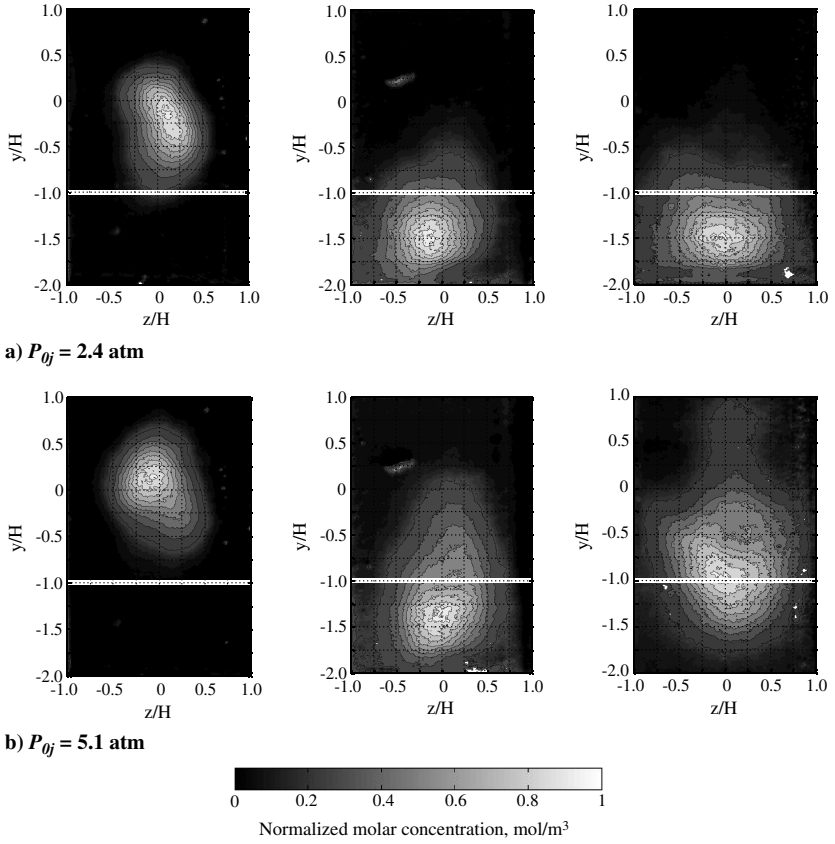

Fig. 8 Averaged end-view PLIF images for He injection with-pylon cases at two different injection pressures: a) $P_{0j} = 2.4$ atm and b) $P_{0j} = 5.1$ atm. Images in planes 1, 2, and 3 are shown from left to right, airflow direction is out of the paper plane, and the injection location is $z/H = 0$ and $x/H = -10$. The solid line at $y/H = -1$ represents the step height.

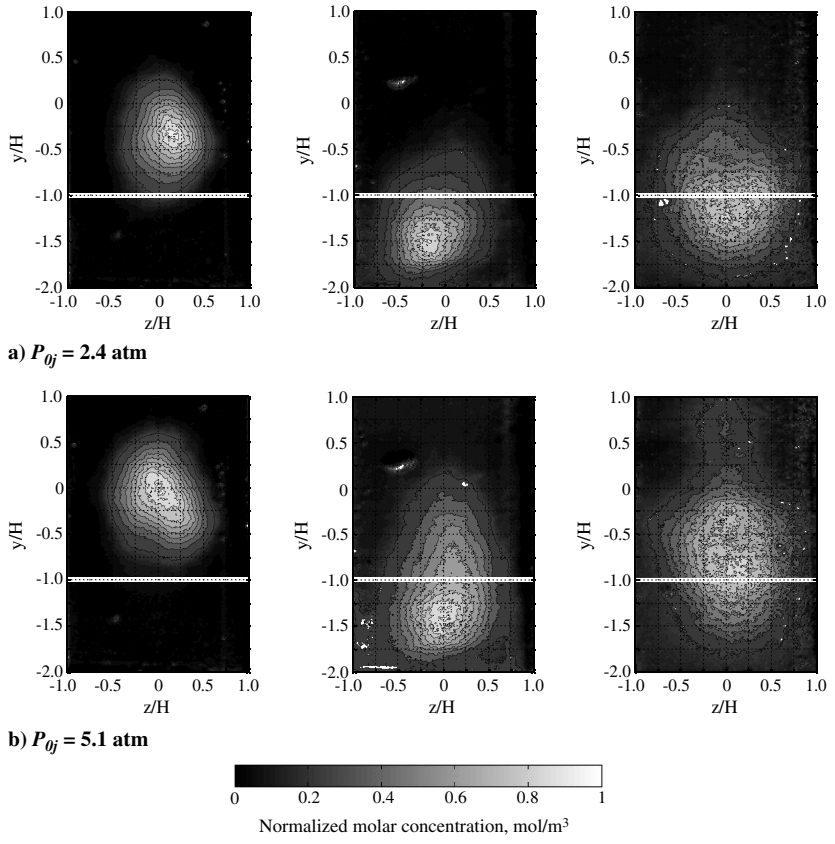

Fig. 9 Averaged end-view PLIF images for Ar injection with-pylon cases at two different injection pressure: a) $P_{0j} = 2.4$ atm and b) $P_{0j} = 5.1$ atm.

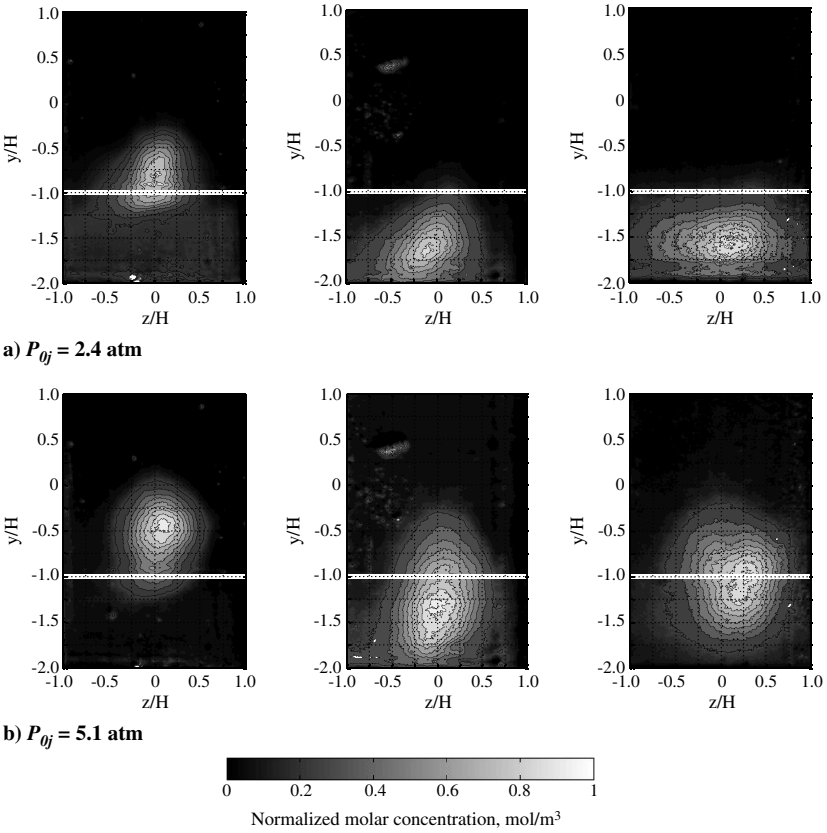

Fig. 10 Averaged end-view PLIF images for He injection without-pylon cases at two different injection pressure: a) $P_{0j} = 2.4$ atm and b) $P_{0j} = 5.1$ atm.

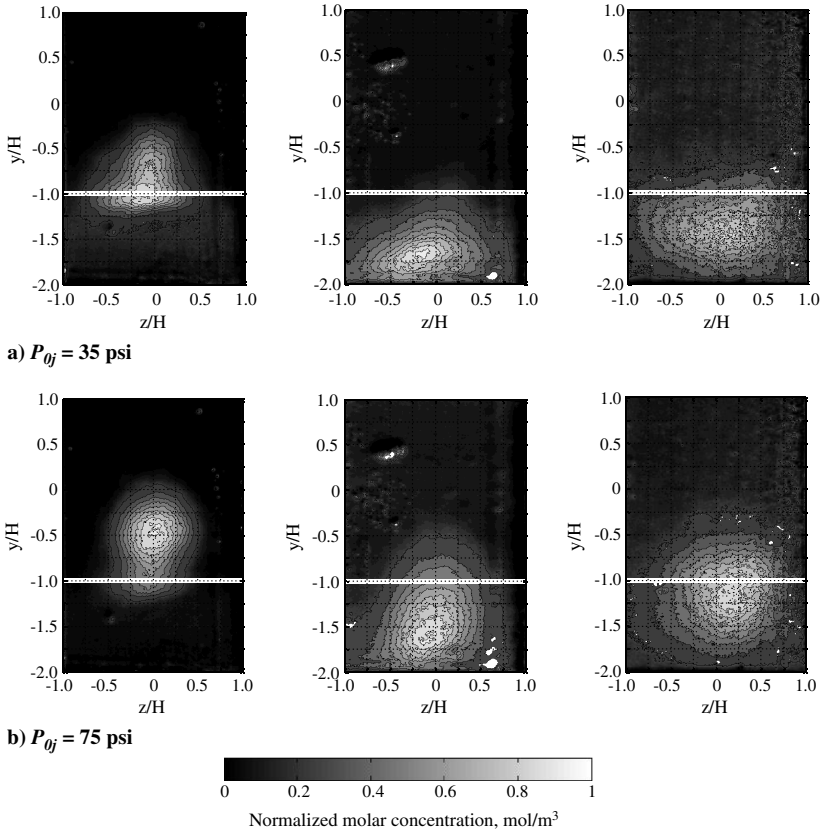

Fig. 11 Averaged end-view PLIF images for Ar injection without-pylon cases at two different injection pressure: a) $P_{0j} = 2.4$ atm and b) $P_{0j} = 5.1$ atm.

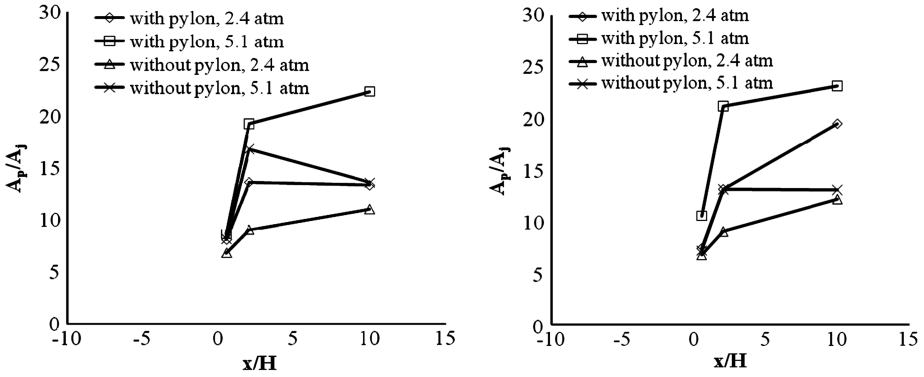

Fig. 12 Plume area comparison for each of four cases along the streamwise direction for a) He and b) Ar. To obtain the area, the pixels within the contour of 30% value of the maximum intensity in each ensemble-averaged image were counted.

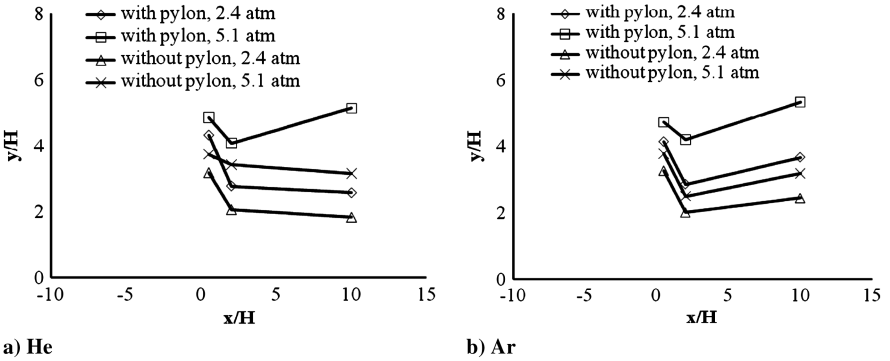

Fig. 13 Plume penetration comparison for each case along the streamwise direction for a) He and b) Ar). The plume penetration was determined by the peak location of the 10% contour of the jet plume.

The computed domain was 340 pixels high by 510 pixels wide for plane 1 and 432 pixels high by 648 pixels wide for plane 3, corresponding to $-2.0 \leq y/H \leq 1.0$ and $-1.0 \leq z/H \leq 1.0$. The spacing used for this correlation covered five pixels, corresponding to $0.029H$ or $0.0046D$ for plane 1 and $0.023H$ or $0.0036D$ for plane 3. This spacing is small enough to resolve the turbulent structure [31].

Figure 15 shows correlation maps for He-injection cases in plane 1. Clearly, the highly correlated region is seen around the reference point. The high correlation region is found around the reference point. For all cases, the negative correlation region, shown in Fig. 15 with gray shades, appears symmetrically to the correlated region, shown with white shades, around the plume center. This indicates that the fluid in the negative region decreases while the fluid around the reference point increases in the given cross section. Since the averaged plume shape suggests the entrainment of the fluid into the step base, this behavior indicates that the fluid in the upper part of the plume displayed as the negative correlation enters into the step base region.

In general, in the pylon cases the highly correlated region is compact and well-organized regardless of the injection pressure. Without the pylon the correlated region is not well organized and expands to the lower region of the duct. These results indicate that there exists a relatively large-scale turbulent structure in this plane and an expectation of enhanced mixing in the step base.

At plane 3 Fig. 16 shows a different trend. In every case the highly correlated region is small. The negatively correlated region that implies the entrainment of fluid in a downward direction is no longer seen, similar to the results in [31]. The region where the large-scale structure is absent has a small correlation region. Therefore, in the

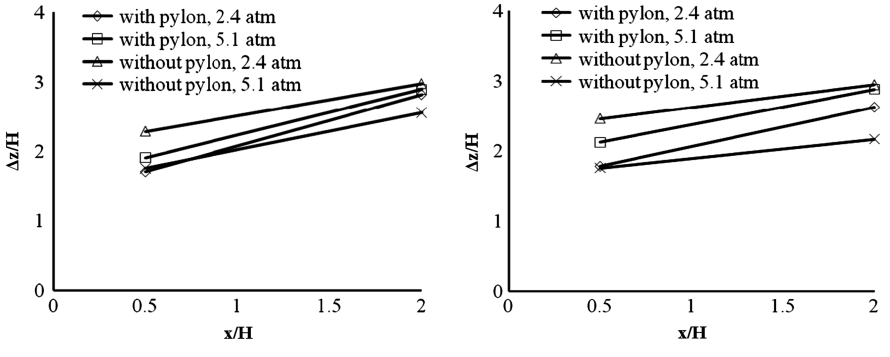

Fig. 14 Plume spreading comparison for each four cases along the streamwise direction for a) He and b) Ar. The lateral spread $\Delta z/H$ was determined from the widest extend of the 10% contour of the jet plume.

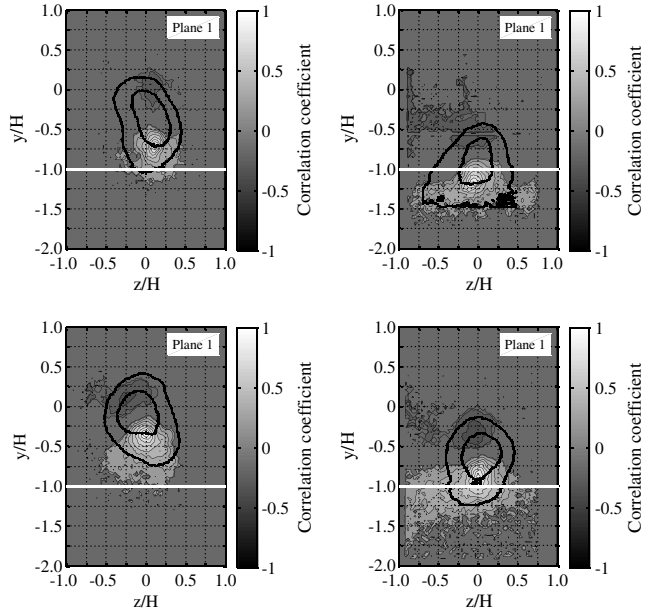

Fig. 15 Correlation maps in plane 1 for He-injection cases: $P_{0j} = 2.4$ atm with pylon (top left), $P_{0j} = 2.4$ atm without pylon (top right), $P_{0j} = 5.1$ atm with pylon (bottom left), and $P_{0j} = 5.1$ atm without pylon (bottom right).

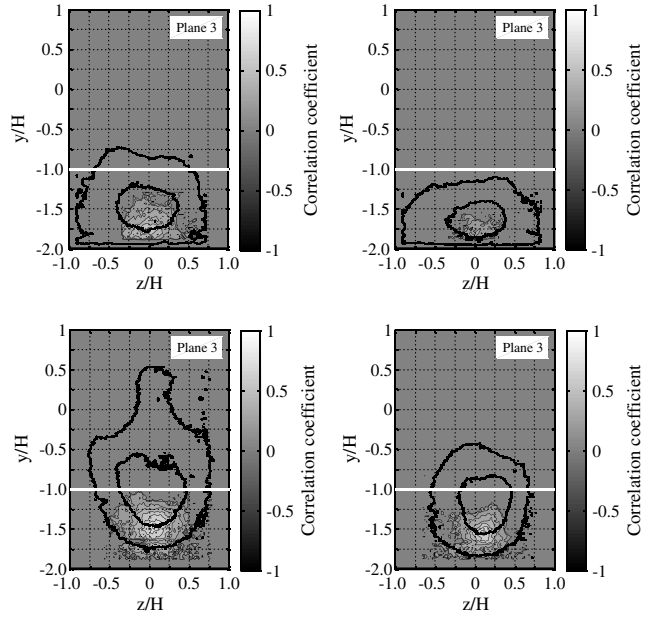

Fig. 16 Correlation maps in plane 3 for He-injection cases: $P_{0j} = 2.4$ atm with pylon (top left), $P_{0j} = 2.4$ atm without pylon (top right), $P_{0j} = 5.1$ atm with pylon (bottom left), and $P_{0j} = 5.1$ atm without pylon (bottom right).

lower-pressure case both with and without the pylon, no large-scale structure seems to exist. In the higher-pressure cases a correlation region appears, but it is considerably smaller than the one met at plane 1.

These observations indicate that at plane 1 the flow is dominated by relatively large-scale turbulent stirring and at plane 3 shear-induced structures are prevalent.

IV. Conclusions

Upstream pylon-aided injection into a Mach 1.6 airstream has been studied using PLIF with data recorded at three planes in a chamber behind a two-dimensional step. Injection pressures and injectants molecular weight were examined with emphasis on penetration, spreading, and shape of the jet plume. The results showed the following:

1) The presence of thin pylon causes essentially no pressure loss.

2) With the pylon all of the jet is lifted from the injection wall with both penetration and spreading increasing. Penetration is increased more at higher injection pressure while spreading dominates at lower injection pressure.

3) Without the pylon the injectant penetration relies only on the injection pressure, but the injectants remain close to the wall, with considerably increased spreading at the lower injection pressure.

4) The injectant molecular weight has little effect on the jet penetration, but the heavier injectant shows increased spreading when the pylon is absent.

5) In the near field the presence of the pylon leads to increased penetration and reduced spreading; however, in the far field spreading is improved by other factors: notably, by the large vortical structures induced by the presence of sidewalls.

6) Statistical analysis conducted for He injection indicated an enhanced dynamic behavior of the flow structure in the near field, represented here by the plane closer to the step.

7) The negative correlation region that appeared symmetrically relative to the plume center indicated that the fluid present in the upper part of the injectant cross section is pushed into the step base region.

8) With the pylon the highly correlated region is compact and well-organized, whereas without the pylon the region is not well organized and expands into the step base.

9) In the far-field plane the highly correlated region is small for every case; this indicates that the large-scale turbulent structure is no longer prevalent in this plane, due to improved mixing in the duct section upstream of the investigated plane.

Acknowledgments

This work has been supported by the U.S. Office of Naval Research. The authors would like to express their gratitude to Gabriel Roy, the Program Manager. Hidemi Takahashi's work has been supported by a Research Fellowship granted by the Japan Society for the Promotion of Science for Young Scientists through grant 20086092. The authors would also like to acknowledge the contributions of Goro Masuya of the Tohoku University in Japan for his support in facilitating the cooperation between the Tohoku University and the University of Florida.

References

[1] Segal, C., *The Scramjet Engine: Processes and Characteristics*, Cambridge Univ. Press, Cambridge, England, U.K., 2009.

[2] Seiner, J. M., Dash, S. M., and Kenzakovich, D. C., "Historical Survey on Enhanced Mixing in Scramjet Engines," *Journal of Propulsion and Power*, Vol. 17, No. 6, 2001, pp. 1273–1286. doi:10.2514/2.5876

[3] Schetz, J. A., Maddalena, L., Throckmorton, R., and Neel, R., "Complex Wall Injector Array for High-Speed Combustors," *Journal of Propulsion and Power*, Vol. 24, No. 4, 2008, pp. 673–680. doi:10.2514/1.36660

[4] Northam, G. B., Greenberg, I., Byington, C. S., and Capriotti, D. P., "Evaluation of Parallel Injector Configurations for Mach 2 Combustion," *Journal of Propulsion and Power*, Vol. 8, No. 2, 1992, pp. 491–499. doi:10.2514/3.23503

[5] Hartfield, R. J., Hollo, S. D., and McDaniel, J. C., "Experimental Investigation of Swept Ramp Injector Using Laser-Induced Iodine Fluorescence," *Journal of Propulsion and Power*, Vol. 10, No. 1, 1994, pp. 129–135. doi:10.2514/3.23721

[6] Riggins, D. W., McClinton, C. R., Rogers, R. C., and Bittner, R. D., "Investigation of Scramjet Strategies for High Mach Number Flows," *Journal of Propulsion and Power*, Vol. 11, No. 3, 1995, pp. 409–418. doi:10.2514/3.23859

[7] Cox, S. K., Fuller, R. P., Schetz, J. A., and Walters, R. W., "Vortical Interaction Generated by an Injector Array to Enhance Mixing in Supersonic Flow," AIAA Paper 94-0708, Jan. 1994.

[8] Fuller, R. P., Wu, P.-K., Nejad, A. S., and Schetz, J. A., "Fuel-Voetrx Interaction for Enhanced Mixing in Supersonic Flow," AIAA Paper 96-2661, July 1996.
[9] Bowersox, R. D. W., "Turbulent Flow Structure Characterization of Angled Injection into a Supersonic Crossflow," *Journal of Propulsion and Power*, Vol. 34, No. 2, 1997, pp. 205–213.
[10] Thomas, R. H., Schetz, J. A., and Fuller, E. J., "Effects of Yaw on Low Angle Injection into a Supersonic Flow," AIAA Paper 1991-14, 1991.
[11] Vinogradov, V. A., and Prudnikov, A. G., "Injection of Liquid into the Strut Shadow at Supersonic Velocities," SAE Aerospace Atlantic Conference, Society of Automotive Engineers, Paper SAE-931455, 1993.
[12] Livingston, T., Segal, C., Schindler, M., and Vingogradov, V. A., "Penetration and Spreading of Liquid Jets in an External-Internal Compression Inlet," *Journal of Propulsion and Power*, Vol. 38, No. 6, 2000, pp. 989–994.
[13] Schetz, J. A., "Injection and Mixing in Turbulent Flow," *Progress in Astronautics and Aeronautics*, edited by M. Summerfield, Vol. 68, AIAA, New York, 1980.
[14] Vinogradov, V. A., Shikhman, Yu. M., and Segal, C., "A Review of Fuel Pre-Injection in Supersonic, Chemically Reacting, Flows," *Applied Mechanics Reviews*, Vol. 60, No. 4, 2007, pp. 139–148. doi:10.1115/1.2750346
[15] Owens, M., Mullagiri, S., Segal, C., and Vinogradov, V. A., "Effects of Fuel Preinjection on Mixing in Mach 1.6 Airflow," *Journal of Propulsion and Power*, Vol. 17, No. 3, 2001, pp. 605–610. doi:10.2514/2.5784
[16] Shikhman, Yu. M., Vinogradov, V. A., Yanovskiy, L. S., Stepanov, V. A., Shlyakotin, V. E., and Penkov, S. N., "The Demonstration of Technologies-Endothermic Hydrocarbon Fueled dual Mode Scramjet," AIAA Paper 2001-1787, 2001.
[17] Vinogradov, V. A., Grachev, V., Petrov, M., and Sheechman, J., "Experimental Investigation of 2-D dual Mode Scramjet with Hydrogen Fuel at Mach 4–6," AIAA Paper 90-5269, 1990.
[18] Guoskov, O. V., Kopchenov, V. I., Lomkov, K. E., Vinogradov, V. A., and Waltrup, P. J., "Numerical Research of Gaseous Fuel Preinjection in Hypersonic Three Dimensional Inlet," *Journal of Propulsion and Power*, Vol. 17, No. 6, 2001, pp. 1162–1169. doi:10.2514/2.5890
[19] Gruber, M. R., Carter, C. D., Montes, D. R., Haubelt, L. C., King, P. I., and Hsu, K.-Y., "Experimental Studies of Pylon-Aided Injection into a Supersonic Crossflow," *Journal of Propulsion and Power*, Vol. 24, No. 3, May–June 2008, pp. 460–470. doi:10.2514/1.32231
[20] Pohlman, M. R., and Greendyke, R. B., "Critical Design Parameters for Pylon-Aided Gaseous Fuel Injection," AIAA Paper 2009-1422, Jan. 2009.
[21] Segal, C., and Young, C. D., "Development of an Experimentally Flexible Facility for Mixing-Combustion Interactions in Supersonic Flow," *Journal of Energy Resources Technology*, Vol. 118, June 1996, pp. 152–158.
[22] Takahashi, H., "Experimental Study of Scalar Structure in a Supersonic Turbulent Mixing Flowfield Using Acetone PLIF," Ph.D. Dissertation, Aerospace Engineering Department, Tohoku Univ., Sendai, Japan, Mar. 2009.
[23] Thurber, M. C., "Acetone Laser-Induced Fluorescence for Temperature and Multiparameter Imaging in Gaseous Flows," Ph.D. Dissertation, Mechanical Engineering Department, Stanford Univ., Stanford, CA, Mar. 1999.
[24] Tu, Q., and Segal, C., "Isolator/Combustion Chamber Interactions During Supersonic Combustion," AIAA Paper 2009-4845, Aug. 2009.
[25] Thakur, A., and Segal, C., "Concentration Distribution in a Supersonic Flow Recirculation Region," *Journal of Propulsion and Power*, Vol. 24, No. 1, Jan. 2008, pp. 64–73. doi:10.2514/1.25396
[26] Ben-Yakar, A., Mungal, M. G., and Hanson, R. K., "Time Evolution and Mixing Characteristics of Hydrogen and Ethylene Transverse Jets in Supersonic Crossflows," *Physics of Fluids*, Vol. 18, 2006, Paper 026101. doi:10.1063/1.2139684
[27] Smith, K. M., and Dutton, J. C., "Investigation of Large-Scale Structures in Supersonic Planar Base Flows," *AIAA Journal*, Vol. 34, No. 6, June 1996, pp. 1146–1152. doi:10.2514/3.13205
[28] Schetz, J. A. and Billig, F. S., "Penetration of Gas Jets Injected into a Supersonic Stream," *AIAA Journal*, Vol. 3, No. 11, Nov. 1966, pp. 1658–1665.
[29] Portz, R., and Segal, C., "Penetration of Gaseous Jets in Supersonic Flows," *AIAA Journal*, Vol. 44, No. 10, Oct. 2006, pp. 2426–2429. doi:10.2514/1.23541
[30] Burger, S. K., Schetz, J. A., and Ungewitter, R., "Effects of Injectant Molecular Weight on Transverse Injection Mixing Processes in Supersonic Flow," AIAA Paper 2009-7315, 2009.
[31] Messersmith, N. L., and Dutton, J. C., "Characteristic Features of Large Structures in Compressible Mixing Layers," *AIAA Journal*, Vol. 34, No. 9, Sept. 1996, pp. 1814–1821. doi:10.2514/3.13312
[32] Takahashi, H., Oso, H., Kouchi, T., Masuya, G., and Hirota, M., "Scalar Spatial Correlations in a Supersonic Mixing Flowfield," AIAA Paper 2009-0023, 2009.

R. Bowersox
Associate Editor